Kinetic nature of hard magnetic $Nd_{50}Al_{15}Fe_{15}Co_{20}$ bulk metallic glass with distinct glass transition

L. Xia[a)]
Institute of Materials, Shanghai University, Shanghai 200072 China; and Institute of Physics, Chinese Academy of Science, Beijing 100080, China

M.B. Tang
Institute of Physics, Chinese Academy of Science, Beijing 100080, China

H. Xu
Institute of Materials, Shanghai University, Shanghai 200072, China

M.X. Pan, D.Q. Zhao, and W.H. Wang
Institute of Physics, Chinese Academy of Science, Beijing 100080, China

Y.D. Dong
Institute of Materials, Shanghai University, Shanghai 200072, China

(Received 6 August 2003; accepted 15 January 2004)

A hard magnetic $Nd_{50}Al_{15}Fe_{15}Co_{20}$ bulk metallic glass (BMG) was prepared in the shape of a rod up to 3 mm in diameter by suction casting. The glass transition and crystallization behaviors as well as their kinetic nature have been studied. In contrast to the previously reported hard magnetic Nd–Al–Fe–Co BMGs, $Nd_{50}Al_{15}Fe_{15}Co_{20}$ as-cast rod exhibits a distinct glass transition and multistep crystallization behaviors in the differential scanning calorimetry traces and lower coercivity. The BMG provides an ideal model for the investigation of glass transition and crystallization of hard magnetic Nd–Al–Fe–Co glass-forming alloys.

Since Croat et al. reported the high coercivity observed in RE–Fe (RE = Nd, Pr) melt-spun ribbon,[1] rare earth–transition metal (RE–TM) metallic glasses with promising magnetic properties have attracted increasing interest because of their great significance in materials science and their considerable technological promise.[2-10] The glass-forming alloys studied include Nd(Pr)–Fe(Co)–Al,[2-8] Nd–Fe–Co–Al–B,[9] Nd(Pr)–Al–Ni–Cu–Fe(Co),[10,11] Y–Fe–Al,[12] and so on. Among these, Nd–Fe(Co)–Al bulk metallic glasses (BMGs) have shown attractive glass-forming ability (GFA), high coercivity, and absence of glass transition temperature in differential scanning calorimetry (DSC) traces.[2-8] Inoue et al. supposed that the high coercivity of the alloys is due to the pre-existence of ferromagnetic clusters, the glass transition temperature might be higher than the crystallization temperature, and the reduced glass transition temperature was estimated to be higher than 0.9.[3] Recent experimental results have shown that the BMGs are partially crystalline,[13] and the absence of glass transition in DSC traces might be due to the chemical inhomogeneity of the amorphous phase.[14] More recently, further results obtained in $Nd_{60}Al_{10}Fe_{20}Co_{10}$ glass-forming alloys have revealed that the typical microstructure of nanoscale particles scattering in the amorphous matrix is closely related to the primary crystallization (observed in the DSC traces of the ribbons) of the alloy,[13,15] and the reduced glass transition temperature representing the GFA might not match the value reported previously.[14,15] Up to now, the glass transition of the alloys can only be obtained in the DSC traces of the paramagnetic $Nd_{60}Co_{30}Al_{10}$ amorphous rods[16] and the partially crystalline $Nd_{60}Al_{10}Co_{30-x}Fe_x$ ($x < 10$) rods.[17] And, it is commonly regarded that both the hard magnetic properties and the absence of glass transition were related to the existence of partially crystalline Nd-Fe–rich clusters.[3,13,14] In this work, we reported the hard magnetic $Nd_{50}Al_{15}Fe_{15}Co_{20}$ bulk metallic glass with distinct glass transition and obvious multistep crystallization behaviors. The BMG provides us an ideal model for investigation of glass transition and crystallization behaviors of Nd–Fe–Co–Al hard magnetic glass-forming alloys.

Ingots with nominal compositions of $Nd_{50}Al_{15}Fe_{15}Co_{20}$ and $Nd_{60}Al_{10}Fe_{20}Co_{10}$ were prepared by arc-melting of 99.9% (at.%) pure Nd, Fe, Al, and Co in a titanium-gettered Ar atmosphere. Cylinders of 3 mm in diameter were prepared by suction casting under argon atmos-

[a)]Address all correspondence to this author.
e-mail: xialei@aphy.iphy.ac.cn
DOI: 10.1557/JMR.2004.0172

phere. The as-cast rod samples were taken from the central region of the cylinders, and the element distribution of the sample was detected to be homogenous within the detection limit of a HITACHI S-570 energy dispersive spectrometer. The structure of the samples was characterized by x-ray diffraction (XRD) in a Philips diffractometer using Cu Kα radiation. The annealing of the rods was performed in a furnace with a vacuum of 2.0×10^{-3} Pa. A vibrating sample magnetometer was used for the magnetic measurements of the as-cast and annealed rods. The field applied was 1432 kA/m. DSC measurements were carried out under a purified argon atmosphere in a Perkin Elmer DSC-7 at heating rates ranging from 10 K/min to 80 K/min. The calorimeter was calibrated for temperature and energy at various heating rates with high-purity indium and zinc. An empty Al pan was first scanned to establish a baseline, and then the same Al pan including the sample was carried out again at the identical thermal condition.

Figure 1(a) shows the XRD pattern of $Nd_{50}Al_{15}Fe_{15}Co_{20}$ as-cast rod. The typical broad diffraction maxima in the XRD pattern show fully amorphous characters of $Nd_{50}Al_{15}Fe_{15}Co_{20}$ as-cast rod within the XRD detection limit. No obvious crystalline peaks were found. The hysteresis loops of the as-cast rod and the rod annealed at 853 K for 5 min are shown in the inset of Fig. 1(a). Similar to $Nd_{60}Al_{10}Fe_{20}Co_{10}$ glass-forming alloy,[13,14] the $Nd_{50}Al_{15}Fe_{15}Co_{20}$ as-cast rod is hard magnetic, whereas the crystalline counterpart is paramagnetic at room temperature. The magnetization (M) at 1432 kA/m of the as-cast sample is 12.8 Am^2/kg while the coercivity (H_c) is 230 kA/m (lower than that of $Nd_{60}Al_{10}Fe_{20}Co_{10}$ as-cast rod[13]). The continuous DSC traces obtained from $Nd_{50}Al_{15}Fe_{15}Co_{20}$ and $Nd_{60}Al_{10}Fe_{20}Co_{10}$ as-cast rods at a heating rate of 10 K/min are shown in Fig. 1(b). There is no glass transition in the DSC trace of $Nd_{60}Al_{10}Fe_{20}Co_{10}$ as-cast rod, and the crystallization behaviors are complicated.[18] In contrast, $Nd_{50}Al_{15}Fe_{15}Co_{20}$ as-cast rod exhibits the endothermic characteristics of a glass transition followed by two exothermic crystallization peaks and a sharp endothermic melting peak. The primary crystallization can also be found in the DSC traces of amorphous $Nd_{57}Al_{10}Fe_{20}Co_5B_8$,[9] $Nd_{60}Fe_{30}Al_{10}$ (30 m/s),[19] and $Nd_{60}Al_{10}Fe_{20}Co_{10}$[13] as-spun ribbons, but it is invisible in the DSC traces of their bulk counterparts. The onset temperatures of the glass transition (T_g), the first crystallization (T_{x1}), the second crystallization (T_{x2}), melting (T_m), and the supercooled liquid region, $\Delta T = T_x - T_g$, are about 487 K, 520 K, 741 K, 788 K, and 33 K, respectively. The reduced glass transition temperature ($T_{rg} = T_g/T_m$) is about 0.62 indicating that the alloy exhibits relatively a large GFA.

To investigate the kinetics of glass transition and crystallization behaviors, DSC measurements of $Nd_{50}Al_{15}Fe_{15}Co_{20}$ as-cast rod were carried out at the heating rates (ϕ) of 10 K/min, 20 K/min, 40 K/min, and 80 K/min, as shown in Fig. 2. The glass transition temperature and crystallization temperatures shift to higher values with increasing heating rates.

The kinetics of the glass transition and crystallizations can be analyzed by the Kissinger equation[20]

$$\ln \frac{T^2}{\phi} = \ln \frac{E}{k_B K_0} + \frac{E}{k_B T} \quad ,$$

where k_B is the Boltzman constant, E is the effective activation energy, and K_0 is the frequency factor in Arreheius law. Figure 3(a) shows the details of glass transition and primary crystallization. The inset illustrates the

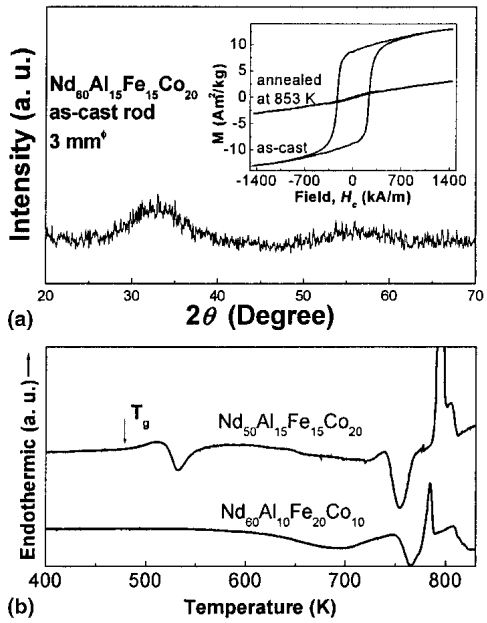

FIG. 1. (a) The XRD pattern of $Nd_{50}Al_{15}Fe_{15}Co_{20}$ as-cast rod. The inset shows the hysteresis loops of as-cast rod and the rod annealed at 853 K for 5 min. (b) The DSC traces of $Nd_{50}Al_{15}Fe_{15}Co_{20}$ and $Nd_{60}Al_{10}Fe_{20}Co_{10}$ as-cast rods at the heating rate of 10 K/min.

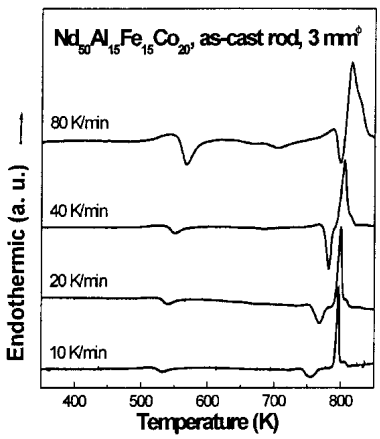

FIG. 2. The DSC traces of $Nd_{50}Al_{15}Fe_{15}Co_{20}$ as-cast rod at the heating rates of 10 K/min, 20 K/min, 40 K/min, and 80 K/min.

linear relations between $\ln(T^2/\phi)$ and $1/T$ for glass transition and primary crystallization. The kinetic characters of the main crystallization are clearly shown in Fig. 3(b). The inset of Fig. 3(b) shows the linear fit between $\ln(T^2/\phi)$ and $1/T$ for the main crystallization. The effective activation energies for glass transition (E_g), primary crystallization (E_{x1}), and secondary crystallization (E_{x2}) were determined by fitting the Kissinger equation to the experimental data. Their values are 2.2 eV, 1.4 eV, and 2.1 eV, respectively.

Concerning the relationship between T_g and $\ln(\phi)$, some authors have observed a Vogel–Fulcher–Tammann type functional dependence.[11,21,22] On the other hand, there are also investigations that reveal the linear increase of T_g with $\ln(\phi)$, especially when the heating rates are not higher than 80 K/min.[23-25] It should be noticed that neglecting the data obtained at higher heating rates (larger than 100 K/min for metallic glass), the measured results at medium heating rates can well fitted to a linear function of T_g versus $\ln(\phi)$,[21-25] and it is argued that T_g obtained at the heating rates larger than 100 K/min are usually lacking accuracy required for DSC measurement.[22] Fecht regarded that thermal measurements can hardly be used to distinguish clearly between Arrhenius and Vogel–Fulcher type behavior.[22] In this work, the dependence of T_g on the heating rates ranging from 10 K/min to 80 K/min follows Lasoka's linear relationship[26]

$$T_g = A + B \ln\phi \quad ,$$

where A and B are constants. The plots of T_g versus $\ln\phi$ are displayed in Fig. 4. A and B for glass transition can be calculated to be 465 and 9. That is, for $Nd_{50}Al_{15}Fe_{15}Co_{20}$ BMG, $T_g = 465 + 9\ln\phi$.

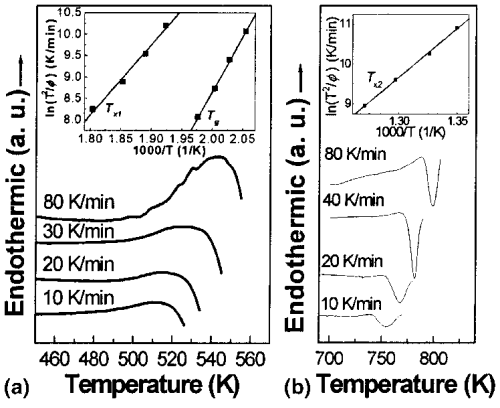

FIG. 3. (a) The details of the glass transition and primary crystallization. The inset shows the linear dependence between $\ln(T^2/\phi)$ and $1/T$ for glass transition and primary crystallization. (b) The details of the main crystallization behavior. In the inset, the line represents the linear fit between $\ln(T^2/\phi)$ and $1/T$ for main crystallization.

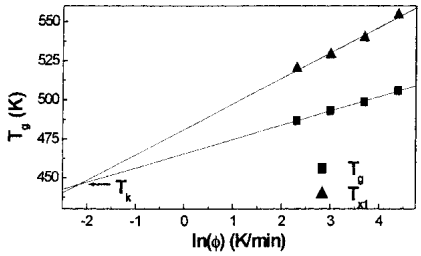

FIG. 4. The linear fit of T_g and T_{x1} versus $\ln\phi$. The extrapolation of two fitted lines intersect at T_K.

Just as the case in $Zr_{41.2}Ti_{13.8}Cu_{12.5}Ni_{10}Be_{22.5}$ BMG and $Cu_{50}Ti_{50}$ amorphous alloys,[25,27] the heating rate dependence of the primary crystallization temperature of $Nd_{50}Al_{15}Fe_{15}Co_{20}$ as-cast rod also follows the Lasocka's relationship as $T_{x1} = 481 + 16\ln(\phi)$, as shown in Fig. 4. The extrapolation of the two fitted lines intersect at a temperature of about 445.5 K. Kauzmann points out that there is an equilibrium temperature (Kauzmann temperature, T_K) at which the entropy of the ideal glass equals to that of the perfect crystals.[28] Crystallization and the ideal glass transition will occur simultaneously at the equilibrium temperature; that is, $T_g = T_{x1} = T_K$. Therefore, the temperature at which the two fitted lines intersected could be the equilibrium temperature of the ideal glass and the perfect crystals. In a nutshell, within experimental error, $T_K = 445.5$ K.

In conclusion, we obtained the hard magnetic $Nd_{50}Al_{15}Fe_{15}Co_{20}$ bulk metallic glass with distinct glass transition and multistep crystallization behaviors. The reduced glass transition temperature (T_{rg}) of the alloy reaches to 0.62 representing excellent glass-forming ability. The effective activation energies for glass transition (E_g), primary crystallization (E_{x1}), and secondary crystallization (E_{x2}) calculated by Kissinger method are 2.2 eV, 1.4 eV, and 2.1 eV, respectively. The dependence of T_g and T_{x1} on the heating rate follows Lasoka's relationship, and the Kauzmann temperature (T_K) is estimated to be 445.5 K.

ACKNOWLEDGMENT

Support by the National Nature Science Foundation of China (Grant Nos. 50031010, 50001007, and 59925101) is gratefully acknowledged.

REFERENCES

1. J.J. Croat, *J. Appl. Phys.* **53,** 3161 (1982).
2. A. Inoue, T. Zhang, W. Zhang, and A. Takeuchi, *Mater. Trans. JIM* **37,** 99 (1996).
3. A. Inoue, A. Takeuchi, and T. Zhang, *Metall. Mater. Trans.* **29A,** 1779 (1998).
4. S. Schneider, A. Bracchi, K. Samwer, M. Seibt, and P. Thiyagarajan, *Appl. Phys. Lett.* **80,** 1749 (2002).
5. J. Ding, Y. Li, and X.Z. Wang, *J. Phys. D* **32,** 713 (1999).

6. G.J. Fan, W. Löser, S. Roth, J. Eckert, and L. Schultz, *J. Mater. Res.* **15,** 1556 (2000).
7. B.C. Wei, Y. Zhang, Y.X. Zhuang, D.Q. Zhao, M.X. Pan, W.H. Wang, and W.R. Hu, *J. Appl. Phys.* **89,** 3529 (2001).
8. B.C. Wei, W.H. Wang, M.X. Pan, B.S. Han, and Z.R. Zhang, *Phys. Rev. B* **64,** 012406 (2001).
9. L.Q. Xing, J. Eckert, W. Löser, S. Roth, and L. Schultz, *J. Appl. Phys.* **88,** 3565 (2000).
10. Y. He, C.E. Price, S.J. Poon, and G.J. Shiflet, Philos. *Mag. Lett.* **70,** 371 (1994).
11. Z.F. Zhao, Z. Zhang, P. Wen, M.X. Pan, D.Q. Zhao, W.H. Wang, and W.L. Wang, *Appl. Phys. Lett.* **82,** 4701 (2003).
12. L. Wang, J. Ding, Y. Li, H.Z. Kong, Y.P. Feng, and X.Z. Wang, *J. Phys. Condens. Matter,* **12,** 4253 (2000).
13. L. Xia, B.C. Wei, Z. Zhang, M.X. Pan, W.H. Wang, and Y.D. Dong, *J. Phys. D* **36,** 775 (2003).
14. B.C. Wei, W. Löser, L. Xia, S. Roth, M.X. Pan, W.H. Wang, and J. Eckert, *Acta Mater.* **50,** 4357 (2002).
15. L. Xia, M.B. Tang, B.C. Wei, M.X. Pan, D.Q. Zhao, W.H. Wang, and Y.D. Dong, *J. Phys. D* **36,** 2954 (2003).
16. A. Inoue and T. Zhang, *Mater. Sci. Eng. A* **226–228,** 393 (1997).
17. G. Kumar, J. Eckert, S. Roth, W. Löser, L. Schultz, and S. Ram, *Acta Mater.* **51,** 229 (2003).
18. L. Xia, B.C. Wei, M.X. Pan, D.Q. Zhao, W.H. Wang, and Y.D. Dong, *J. Phys. Condens. Matter* **15,** 3531 (2003).
19. X.Z. Wang, Y. Li, J. Ding, L. Si, and H.Z. Kong, *J. Alloys Comp.* **290,** 209 (1999).
20. H.E. Kissinger, *J. Res. Natl. Bur. Stand.* **57,** 217 (1956).
21. N. Mitrovic, S. Roth, and J. Eckert, *Appl. Phys. Lett.* **78,** 2145 (2001).
22. H.J. Fecht, *Mater. Trans. JIM* **36,** 777 (1995).
23. Y.X. Zhuang, W.H. Wang, Y. Zhang, M.X. Pan, and D.Q. Zhao, *Appl. Phys. Lett*. **75,** 2392 (1999).
24. Y.X. Zhuang and W.H. Wang, *J. Appl. Phys.* **87,** 8209 (2000).
25. R. Busch, Y.J. Kim, and W.L. Iohnson, *J. Appl. Phys.* **77,** 4093 (1995).
26. M. Lasocka, *Mater. Sci. Eng*. **23,** 173 (1976).
27. C.H. Hwang, S. Kang, K. Cho, and K. Kawamura, *Scr. Metall.* **19,** 1403 (1985).
28. W. Kauzmann, *Chem. Rev.* **43,** 219 (1948).